Symmetric Infinite Impulse Response filtering: methods and application on ocean inertial waves

Damien Allain

Symmetric Infinite Impulse Response filtering: methods and application on ocean inertial waves

Damien J. Allain[1]

[1]CNRS, LEGOS (UMR5566 CNRS-CNES-IRD-UPS), France

2014/07/08

Acronyms

IW Inertial Wave
CF Coriolis Frequency
NDR Number of Delay Registers
DF Direct-Form
IIR Infinite Impulse Response
BP Band-Pass
BC Band-Cut
SBP Symmetric Band-Pass
SBC Symmetric Band-Cut
RMS Root Mean Square

Abstract

Symmetric Infinite Impulse Response (IIR) filters have been designed to filter geophysical time series, in particular to remove the signature of Inertial Waves (IWs) as it is often so strong it disturbs the observations and analyses of other phenomena. As the symmetric filters are based on IIR digital filters, their computational costs are reduced to a minimum and their parameters can be adapted to all latitudes when used on IWs. The Symmetric Band-Cut (SBC) filter has been tested. The results show that the SBC filter can remove a lot of the signal from IWs but that a good understanding of the filter is necessary to interpret its output, as it shows transition and boundary effects. For that reason, a synthetic case has been presented to enable users to get the best understanding of the filter.

1 Introduction

Inertial Waves (IWs) are described by e.g. Millot (1990, sec.6).

IWs have a frequency spectrum that is spread around the Coriolis Frequency (CF). In this article, the CF at will be noted with the latitude as subscript: at a latitude of ϕ the CF is ω_ϕ. Taking Ω the spinning frequency of the Earth gives:

$$\omega_\phi = 2\Omega \sin \phi \tag{1a}$$

In an even simpler way, taking ω_{K2} the average frequency of the K2 tidal wave gives:

$$\omega_\phi = \omega_{K2} \sin \phi \tag{1b}$$

This means:

$$0 \leq \omega_\phi \leq \omega_{K2} \tag{2}$$

IWs can have a strong signature on analysed parameters, e.g. with water velocity at or near the surface of the deap ocean. This signature is often so strong it disturbs the observations and analyses of other phenomena. For an example, see Petrenko et al. (2008).

Filtering out the signature of IWs is very different from removing the tidal signature. Tides can also have a strong signature on analysed parameters. This signature is also often so strong it disturbs the observations and analyses of other phenomena. Thankfully tides have an almost discrete frequency spectrum. So a frequency analysis will give the amplitudes and phases of the frequency constituents. From these a prediction can be computed. Subtracting this prediction removes the tidal signature. This is called detiding.

Unlike tides, the frequency spectrum of IWs is continuous: it has an infinite number of constituents. This means the only way to remove or attenuate the signature of IWs is filtering out their frequency domain from the signal.

In sec. 2 a base type of digital filter will be chosen and its basic characteristics will be studied. In sec. 3, its main limitation for its use for, at least, geophysical applications will be addressed giving a final type of filter. In sec. 4 the results of a test of the filter on real data will be presented.

2 Filter choices

2.1 Type

It is currently common to take a convolution kernel to carry out filtering in oceanography. An example is the Demerliac (1974) filter, whose convolution kernel spans 72 hours. With ever-increasing resolutions, we are currently reaching a point at which simulations on a grid of $40{\cdot}10^6$ vertexes (for example on a $10^3 \times 10^3 \times 40$ grid) or more are common place. A 72 steps filter on such a grid would require $72 \times 40{\cdot}10^6 \simeq 3{\cdot}10^9$ multiplications per time step and, coding numbers with 8 B double precision type, would take more than 23 GB of memory, which is currently feasible, but still quite a challenge. It will also be shown, e.g. in sec. 2.3.3, that an appropriate filter for IWs can take several hundreds of elements. So, because of its need in memory and its cost in computation, a convolution kernel is not practical for filtering the signature of IWs.

But digital filtering is not limited to convolution. In particular, an Infinite Impulse Response (IIR) filter can be chosen because it can have a very large convolution kernel with a very limited Number of Delay Registers (NDR). For simplicity, Direct-Form (DF) IIR filters are chosen. There are two type of DF IIR filters. DF-I IIR filters do not have an internal register that is vulnerable to overflow when using fixed-point calculation (Smith, 2007), but have a NDR that is twice the order. As floating-point calculation is used here, and in order to limit further the NDR, a DF-II IIR filter, whose NDR is the same as the order of the filter, is chosen.

As geophysicists are not all familiar with IIR filters, mainly used in electronics, a lot of relevant details will be given. In sec. 2.2 the set-up of the DF-II IIR filter will be detailed. Because the Band-Pass (BP) filter is so complementary to the Band-Cut (BC) filter that understanding the characteristics of the BP filter helps understanding the characteristics of the BC filter, both BP and BC filters will be presented. In sec. 2.3 and 2.4 the parameters of, respectively, the BP and BC filters will be calculated. In sec. 2.5 the phase shift and its importance will be exposed.

2.2 Order

Taking $z = e^{j\omega s^{-1}}$ the transfer function of a 1 step advance with s the sampling frequency, we have the diagram of second-order DF-II IIR filter on fig. 1. The input I is fed to an adder.

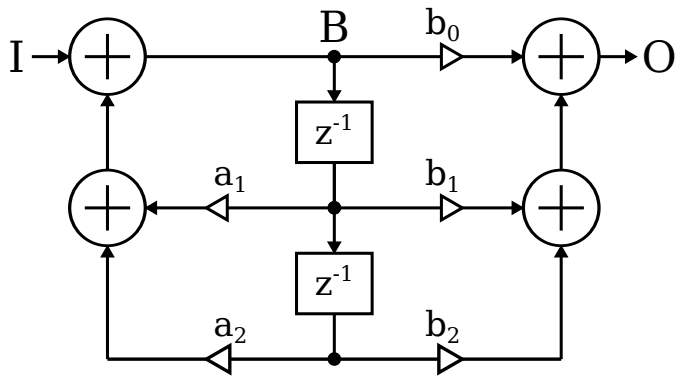

Figure 1: Second-order DF-II IIR filter, from Smith (2007, fig.9.2)

The output B of this adder is connected to the input of the first delay register. The filter has 2 cascaded delay registers. The outputs of the delay registers are not only multiplied by b_1 and b_2 and added to B, itself multiplied by b_0, to give the output O but also multiplied by a_1 and a_2 and added to I to give B. This gives, for every element n of the input I, the intermediate value B and the output O:

$$\begin{aligned} B_n &= I_n + a_1 B_{n-1} + a_2 B_{n-2} && \text{(3a)} \\ O_n &= b_0 B_n + b_1 B_{n-1} + b_2 B_{n-2} && \text{(3b)} \\ &= b_0 \left(I_n + a_1 B_{n-1} + a_2 B_{n-2}\right) + b_1 B_{n-1} + b_2 B_{n-2} && \text{(3c)} \end{aligned}$$

This feed-back makes the response of the filter infinite.

Eq. (3) gives the frequency transforms of I, B and O:

$$\begin{aligned} F(B) &= F(I) + F(B)\left(a_1 z^{-1} + a_2 z^{-2}\right) && \text{(4a)} \\ \Leftrightarrow F(B) &= F(I)\frac{1}{1 - a_1 z^{-1} - a_2 z^{-2}} && \text{(4b)} \\ F(O) &= F(B)\left(b_0 + b_1 z^{-1} + b_2 z^{-2}\right) && \text{(4c)} \end{aligned}$$

which gives the transfer function $H(\omega)$:

$$H(\omega) = \frac{b_0 + b_1 z^{-1} + b_2 z^{-2}}{1 - a_1 z^{-1} - a_2 z^{-2}} \tag{4d}$$

We are now left with the choice of constants to tune the filter to our needs.

2.3 Band-Pass

2.3.1 Constants

For a BP transfer function H_p, we need, with $z_0 = e^{j\omega_0 s^{-1}}$ and $\omega_s = \omega_0 s^{-1}$:

$$\begin{cases} H_p(0) &= 0 \\ H_p(\pi s) &= 0 \\ H_p(\omega_0) &= 1 \end{cases} \Leftrightarrow \begin{cases} b_0 & +b_1 & +b_2 &= & 0 \\ b_0 & -b_1 & +b_2 &= & 0 \\ b_0 & +b_1 z_0^{-1} & +b_2 z_0^{-2} &= & 1 - a_1 z_0^{-1} - a_2 z_0^{-2} \end{cases} \tag{5a}$$

$$\Leftrightarrow \begin{cases} b_1 & +b_2 & & & = & -b_0 \\ -b_1 & +b_2 & & & = & -b_0 \\ b_1\cos\omega_s & +b_2\cos 2\omega_s & +a_1\cos\omega_s & +a_2\cos 2\omega_s & = & 1-b_0 \\ -b_1\sin\omega_s & -b_2\sin 2\omega_s & -a_1\sin\omega_s & -a_2\sin 2\omega_s & = & 0 \end{cases} \tag{5b}$$

$$\Leftrightarrow \begin{cases} b_1 & & & = & 0 \\ b_2 & & & = & -b_0 \\ -b_0\cos 2\omega_s & +a_1\cos\omega_s & +a_2\cos 2\omega_s & = & 1-b_0 \\ b_0\sin 2\omega_s & -a_1\sin\omega_s & -a_2\sin 2\omega_s & = & 0 \end{cases} \tag{5c}$$

which, when $\sin\omega_s\cos 2\omega_s - \cos\omega_s\sin 2\omega_s = \sin(\omega_s - 2\omega_s) = -\sin\omega_s \neq 0$, gives:

$$\begin{cases} b_0 & = & b_p \\ b_1 & = & 0 \\ b_2 & = & -b_p \\ a_1 & = & 2\left(1-b_p\right)\cos\omega_s \\ a2 & = & 2b_p - 1 \end{cases} \tag{5d}$$

or:

$$\begin{aligned} H_p(\omega) &= \frac{b_p - b_p z^{-2}}{1 - a_1 z^{-1} - a_2 z^{-2}} = \frac{b_p\left(1-z^{-2}\right)}{1 - a_1 z^{-1} - a_2 z^{-2}} \\ &= \frac{b_p\left(z - z^{-1}\right)}{z - \left(1-b_p\right)\left(z_0 + z_0^{-1}\right) - \left(2b_p - 1\right) z^{-1}} \end{aligned} \tag{5e}$$

2.3.2 Responses

The convolution kernel is obtained by computing the impulse response. As both the convolution kernel and the impulse response are equivalent, both terms will be used when describing this feature of the filters presented in this article.

The amplitude and phase diagrams and the convolution kernel are shown on fig. 2 for different values of b_p. The amplitude and phase diagrams show the specifications of the BP filter, given in eq. (9a), are respected. The amplitude diagram shows that, the lower b_p is, the sharper the filter is. The phase diagram shows that when $\omega \to 0$ the phase tends to $\pi/2$ and that when $\omega \to 2\pi s$ the phase tends to $-\pi/2$. It also shows that the lower b_p is, when ω decreases or increases from ω_0, the faster the phase will go towards $\pi/2$ or $-\pi/2$. The impulse response diagram shows slowly decaying reponses. It also shows that the lower b_p is, the slower the decay is. For higher values of b_p, the impulse reponses show oscillations.

2.3.3 Quality factor

Fig. 2 shows the convolution kernel can be very wide. Estimating the width of the convolution kernel is important in order to take properly into account the contribution of the last elements of the input. For this, both definitions of the quality factor Q are used. We have indeed, with $\Delta\omega$ the bandwidth:

$$Q = \frac{\Delta\omega}{\omega_0} \tag{6a}$$

and also, with E the energy contribution of an element of the input and t the amount of time since that element occurred, derived from Smith (2007, Quality Factor):

$$Q = \omega_0 E \frac{\partial t}{\partial E} \tag{6b}$$

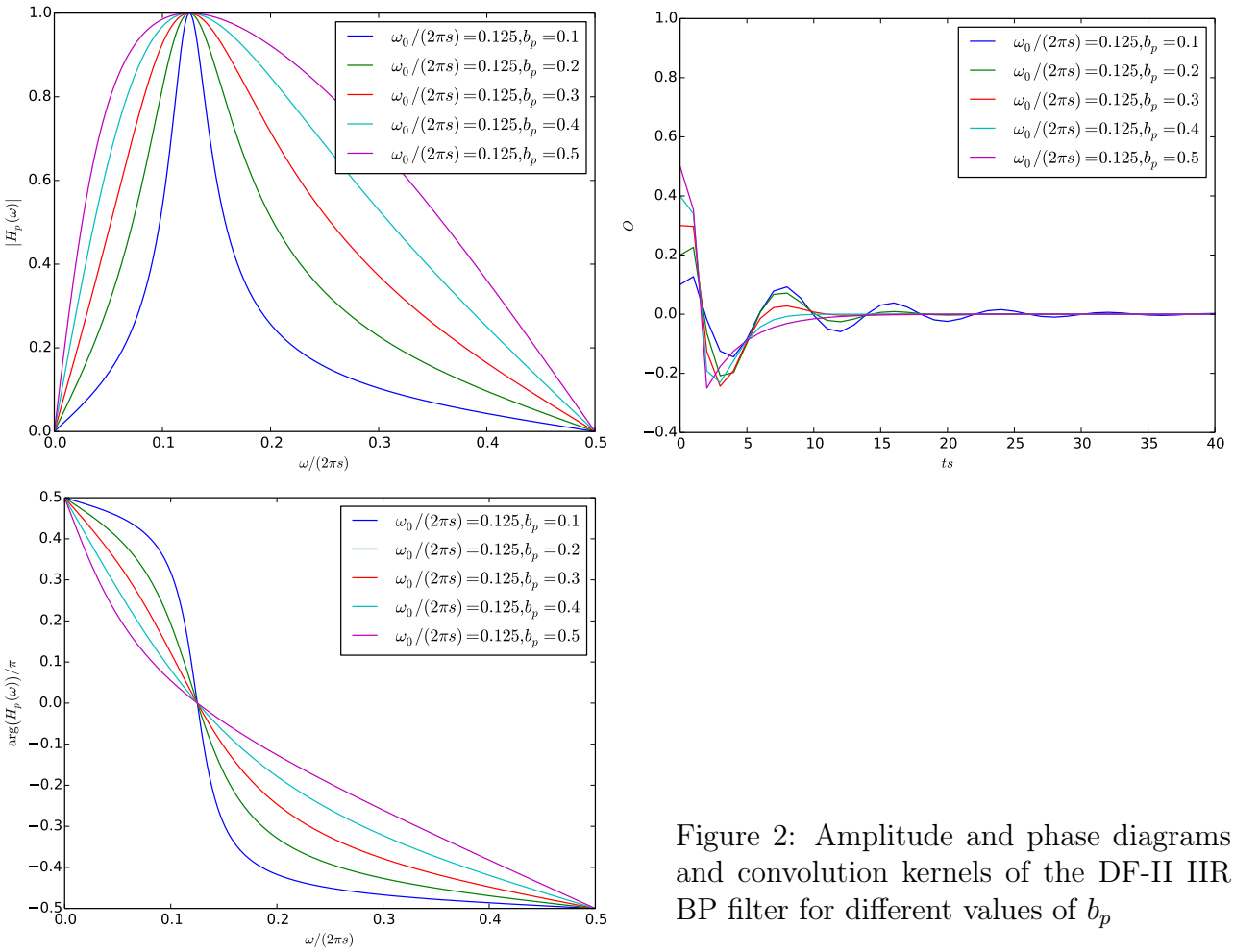

Figure 2: Amplitude and phase diagrams and convolution kernels of the DF-II IIR BP filter for different values of b_p

$$E \propto \exp\left(-t\frac{\omega_0}{Q}\right) \tag{6c}$$

If we want 99.9% of the contribution of the last element, we must take an extra l steps:

$$l = -\ln 10^{-3}\frac{Q}{\omega_0}s \simeq 7\frac{Q}{\omega_0}s = 7\frac{\Delta\omega}{\omega_0^2}s \tag{6d}$$

We can approximate $\Delta\omega$ by deriving the transfer function around the peak, taking $\epsilon = js^{-1}\partial\omega$:

$$\begin{aligned}
z+\partial z &= z + js^{-1}z\partial\omega = z(1+\epsilon)\\
z^{-1}+\partial z^{-1} &= z^{-1} - js^{-1}z^{-1}\partial\omega = z^{-1}(1-\epsilon)\\
H(\omega_0+\partial\omega) &= \frac{b_p\left(z_0(1+\epsilon) - z_0^{-1}(1-\epsilon)\right)}{z_0(1+\epsilon) - (1-b_p)\left(z_0+z_0^{-1}\right) - (2b_p-1)\,z_0^{-1}(1-\epsilon)}\\
&= \frac{b_p\left(z_0 - z_0^{-1} + \epsilon(z_0+z_0^{-1})\right)}{z_0+\epsilon z_0 - z_0 - z_0^{-1} + b_p\left(z_0+z_0^{-1}\right) - 2b_p z_0^{-1} + 2b_p\epsilon z_0^{-1} + z_0^{-1} - \epsilon z_0^{-1}}\\
&= \frac{b_p\left(z_0 - z_0^{-1} + \epsilon(z_0+z_0^{-1})\right)}{\epsilon z_0 + b_p\left(z_0 - z_0^{-1}\right) + 2b_p\epsilon z_0^{-1} - \epsilon z_0^{-1}}\\
&= \frac{b_p\left(z_0 - z_0^{-1} + \epsilon(z_0+z_0^{-1})\right)}{\left(z_0 - z_0^{-1}\right)(b_p+\epsilon) + 2b_p\epsilon z_0^{-1}} = \frac{z_0 - z_0^{-1} + \epsilon\left(z_0+z_0^{-1}\right)}{z_0 - z_0^{-1} + \epsilon b_p^{-1}\left(z_0 - z_0^{-1}\right) + 2\epsilon z_0^{-1}}\\
&= \frac{2j\sin\omega_s + 2\epsilon\cos\omega_s}{2j\sin\omega_s + 2j\epsilon b_p^{-1}\sin\omega_s + 2\epsilon z_0^{-1}} = \frac{\sin\omega_s - j\epsilon\cos\omega_s}{\sin\omega_s + \epsilon b_p^{-1}\sin\omega_s - j\epsilon z_0^{-1}}
\end{aligned} \tag{7a}$$

$$
\begin{aligned}
H(\omega_0+\partial\omega) &= \frac{\sin\omega_s + s^{-1}\cos\omega_s\partial\omega}{\sin\omega_s + s^{-1}\left(jb_p^{-1}\sin\omega_s + z_0^{-1}\right)\partial\omega} \\
&= \frac{\sin\omega_s + s^{-1}\cos\omega_s\partial\omega}{\sin\omega_s + s^{-1}\left(jb_p^{-1}\sin\omega_s + \cos\omega_s - j\sin\omega_s\right)\partial\omega} \qquad (7b)
\end{aligned}
$$

$$
|H(\omega_0+\partial\omega)| = \sqrt{\frac{\left[\sin\omega_s + s^{-1}\cos\omega_s\partial\omega\right]^2}{\left[\sin\omega_s + s^{-1}\cos\omega_s\partial\omega\right]^2 + \left[s^{-1}\sin\omega_s\left(b_p^{-1}-1\right)\partial\omega\right]^2}} \qquad (7c)
$$

as $\partial\omega \to 0$:

$$
|H(\omega_0+\partial\omega)| \to 1 - \frac{\left[s^{-1}\sin\omega_s\left(b_p^{-1}-1\right)\partial\omega\right]^2}{\left[\sin\omega_s\right]^2} \to 1 - 2^{-1}\left[s^{-1}\left(b_p^{-1}-1\right)\partial\omega\right]^2 \qquad (7d)
$$

when $b_p \to 0$:

$$
|H(\omega_0+\partial\omega)| \to 1 - \left[\frac{\partial\omega}{4b_p s}\right]^2 \qquad (7e)
$$

from which we can approximate the quality factor:

$$
Q \simeq \frac{w_0}{2b_p s} \qquad (8a)
$$

which is given in most electronics text books but I did not find its derivation, as in (7), in the many ones I searched in. It gives the following simple relation for 99.9% contribution:

$$
l \simeq 7b_p^{-1} \qquad (8b)
$$

It will be shown in sec. 4 that, for applications on IWs, we can have $b_p \ll 0.07$, making $l \gg 100$, which is particularly large for a convolution kernel.

2.4 Band-Cut

2.4.1 Constants

For a BC transfer function, we need, with $z_0 = e^{j\omega_0 s^{-1}}$ and $\omega_s = \omega_0 s^{-1}$:

$$
\begin{cases} H_c(\omega_0) = 0 \\ H_c(0) = 1 \\ H_c(\pi s) = 1 \end{cases} \Leftrightarrow \begin{cases} b_1\cos\omega_s & +b_2\cos 2\omega_s & & & = & -b_0 \\ -b_1\sin\omega_s & -b_2\sin 2\omega_s & & & = & 0 \\ b_1 & +b_2 & +a_1 & +a_2 & = & 1-b_0 \\ -b_1 & +b_2 & -a_1 & +a_2 & = & 1-b_0 \end{cases} \qquad (9a)
$$

which, when $\sin\omega_s\cos 2\omega_s - \cos\omega_s\sin 2\omega_s = \sin(\omega_s - 2\omega_s) = -\sin\omega_s \neq 0$, gives:

$$
\begin{cases} b_0 = b_c \\ b_1 = -2b_c\cos\omega_s \\ b_2 = b_c \\ a_1 = -b_1 = 2b_c\cos\omega_s \\ a_2 = 1-2b_c \end{cases} \qquad (9b)
$$

or:

$$
\begin{aligned}
H_c(\omega) &= \frac{b_c + b_1 z^{-1} + b_c z^{-2}}{1 + b_1 z^{-1} - a_2 z^{-2}} = \frac{b_c z + b_1 + b_c z^{-1}}{z + b_1 - a_2 z^{-1}} \\
&= \frac{b_c\left(z + z^{-1} - z_0 - z_0^{-1}\right)}{z - b_c\left(z_0 + z_0^{-1}\right) - \left(1-2b_c\right)z^{-1}} \qquad (9c)
\end{aligned}
$$

Taking $b_c = 1 - b_p$ gives:

$$\begin{aligned} H_c(\omega) &= \frac{(1-b_p)\left(z + z^{-1} - z_0 - z_0^{-1}\right)}{z - (1-b_p)\left(z_0 + z_0^{-1}\right) - (2b_p - 1)\, z^{-1}} \\ &= 1 - \frac{z - (1-b_p)\left(z_0 + z_0^{-1}\right) - (2b_p - 1)\, z^{-1} - (1-b_p)\left(z + z^{-1} - z_0 - z_0^{-1}\right)}{z - (1-b_p)\left(z_0 + z_0^{-1}\right) - (2b_p - 1)\, z^{-1}} \\ &= 1 - \frac{b_p\,(z - z^{-1})}{z - (1-b_p)\left(z_0 + z_0^{-1}\right) - (2b_p - 1)\, z^{-1}} \\ &= 1 - H_p(\omega) \end{aligned} \tag{9d}$$

which shows that the BC filter is the complement of the BP filter.

2.4.2 Responses

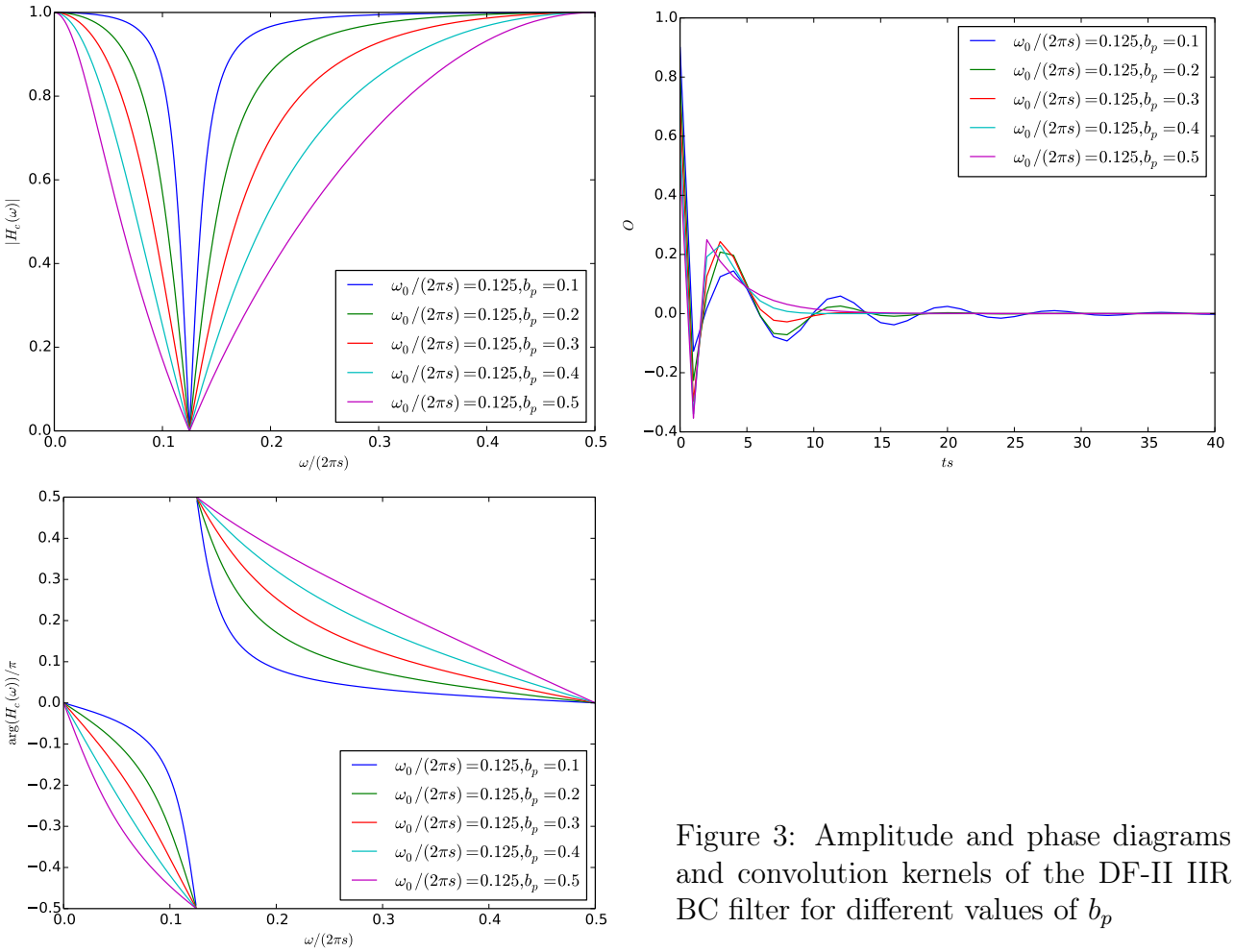

Figure 3: Amplitude and phase diagrams and convolution kernels of the DF-II IIR BC filter for different values of b_p

The amplitude and phase diagrams and the convolution kernel are shown on fig. 3 for different values of b_c. The amplitude and phase diagrams show the specifications of the BC filter, given in eq. (9a), are respected. The amplitude diagram shows that, the lower b_p is, the sharper the filter is. It must also be noted that the derivative around the minimum is not 0. This means the filter will have an important leak around its cut frequency. The phase diagram shows that when $\omega \to \omega_0$ the phase tends to $-\pi/2$ when $\omega < \omega_0$ and to $\pi/2$ when $\omega > \omega_0$. It also shows that the lower b_p is, when ω decreases or increases from ω_0, the faster the phase will go towards 0. The impulse response diagram shows the response is the exact difference between

the impulse itself and the impulse response of the BP filter, again showing that the BC filter is the complement of the BP filter. So, for the same value of b_p, the width of the convolution kernel of the BC filter is the same as that of the BP filter.

2.5 Phase shifts

It must be highlighted that the filters described in the previous sections have a phase shift. Indeed their impulse responses are not symmetric.

This is not relevant in the case of a spectral analysis, where the output will only be the amount of energy in a frequency band. Such analyses are of interest, e.g. in the search of a cause of an error known to be around a certain frequency.

3 Symmetric filtering

However filtering without phase shift is necessary (Demerliac, 1974). This means the transfer function only has a real part. This can be done by multiplying it with its complex conjugate:

$$\overline{H(\omega)} = \frac{b_0 + b_1 z + b_2 z^2}{1 - a_1 z - a_2 z^2} \tag{10}$$

Eq. (10) shows this can be done by running the filter again with, as its input, the reversed output of the previous filter run. This can also be found intuitively: a reverse filter run will shift whatever has been shifted one way back the other way. It is therefore only possible during post-processing. Users who wish to remove the signature of a signal with a certain frequency spectrum on sub-sampled outputs must be reminded to filter the aliased spectrum, and so to also filter whatever else was at that aliased spectrum before aliasing.

The frequency and impulse responses diagrams of the SBP and the SBC filters are shown on fig. 4 for different values of b_p. The frequency response of a symmetric filter is just the square of the amplitude response of its base filter. So, again, the frequency response diagrams show that, the lower b_p is, the sharper the filters are. The impulse response diagram show the response of the SBC is the exact difference between the impulse itself and the impulse response of the SBP filter. The frequency response diagrams also show the frequency response of the SBC is the exact difference between 1 and the frequency response of the SBP filter. So both types of diagrams show that the SBC filter is the complement of the SBP filter. It must also be noted that the derivative around the minimum is 0 for both filters. This means that, unlike the BP filter, the SBP filter will not have an important leak around its cut frequency making it more efficient at removing signals with a continous spectrum like IWs. The impulse responses diagrams show that this time the impulses reponses are symmetric around 0. Again the impulse response diagrams show slowly decaying reponses, but this time the decay are on both sides of the center. They also again show that the lower b_p is, the slower the decays are. The impulse reponses show again oscillations for higher values of b_p, actually for the very same values of b_p for which the base filters show oscillations themselves.

4 Test results

4.1 Model output

In order to illustrate the behaviour of these filters on real data, an example was taken from a model run in the Bay of Biscay. The model used was SYMPHONIE version S-2010.17. The run was carried out by Herbert (2012, sec.III.1.II) to study the response of the ocean to the

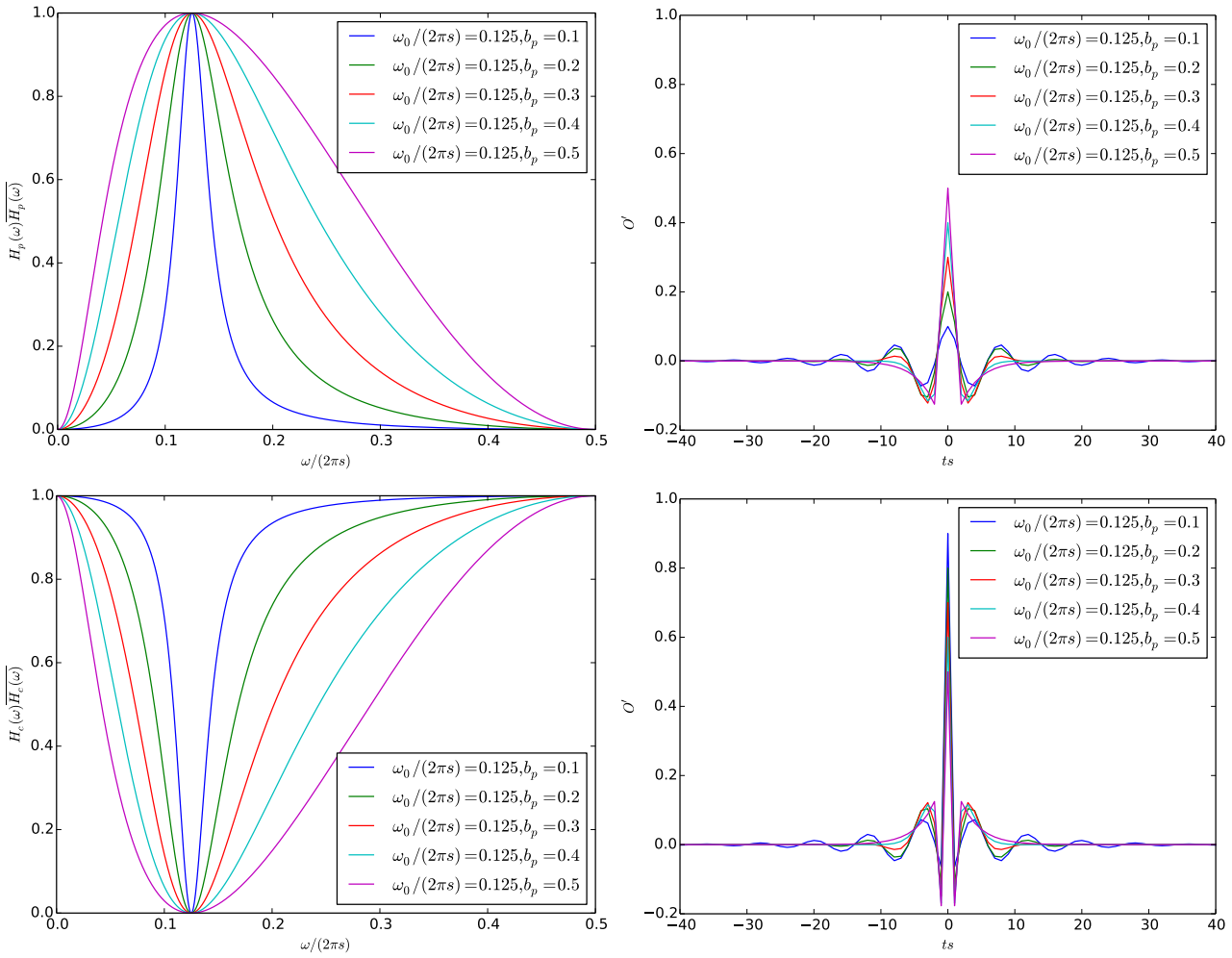

Figure 4: Frequency (left) and impulse (right) responses diagrams of the DF-II IIR SBP (top) and SBC (bottom) filters for different values of b_p

Klaus storm on 23 to 24 Jan 2009. Its grid has 362×370 tracer points and 43 levels, so more than $3.9{\cdot}10^6$ values per parameter per time frame. The saved output has an hourly sampling and spans from 1 Dec 2008 00:00 to 28 Feb 2009 00:00, so also covers the days of the Quinten storm on 9 Feb 2009. The first 15 days were remove from this analysis as spin-up time.

The most relevant data point was searched by running a spectral analysis of the sea water velocity components by taking the Root Mean Square (RMS) of the output of a BP filter taking, with a latitude between 43° and 51°, between 17.5h or $20.5°h^{-1}$ and 15.4h or $23.4°h^{-1}$ therefore centred around 16.5h or $21.8°h^{-1}$ with a quality factor of 16. The treatment took around 6min for each components.

A set of frames, covering the period of IWs, of the filtered output are shown on fig. 5. Comparing the directions between the first frame (1440) and the other frames gives the period of the oscillations. On the continental shelf, i.e. north of a line going through 44N 2W, 46N 4W and 48N 8W, the arrows show the directions have a period around 12.5h (frames 1452 and 1453). This shows the dominant signal in this area, even after filtering, remains the diurnal tides. In the deep ocean the directions have the inertial period around 16.5h (frames 1452 and 1453). All the frames also show that the norm of the velocity remains the same from frame to frame. This shows the particles of water are just moving in circles. The maximum speed being around $0.15\,\mathrm{m\,s^{-1}}$, the circles are up to around 1.4km in diameter.

The results of the analysis are shown on fig. 6. Data on the continental shelf is discarded from this study as signal from the strong tide leaked through the filter. So only the deep

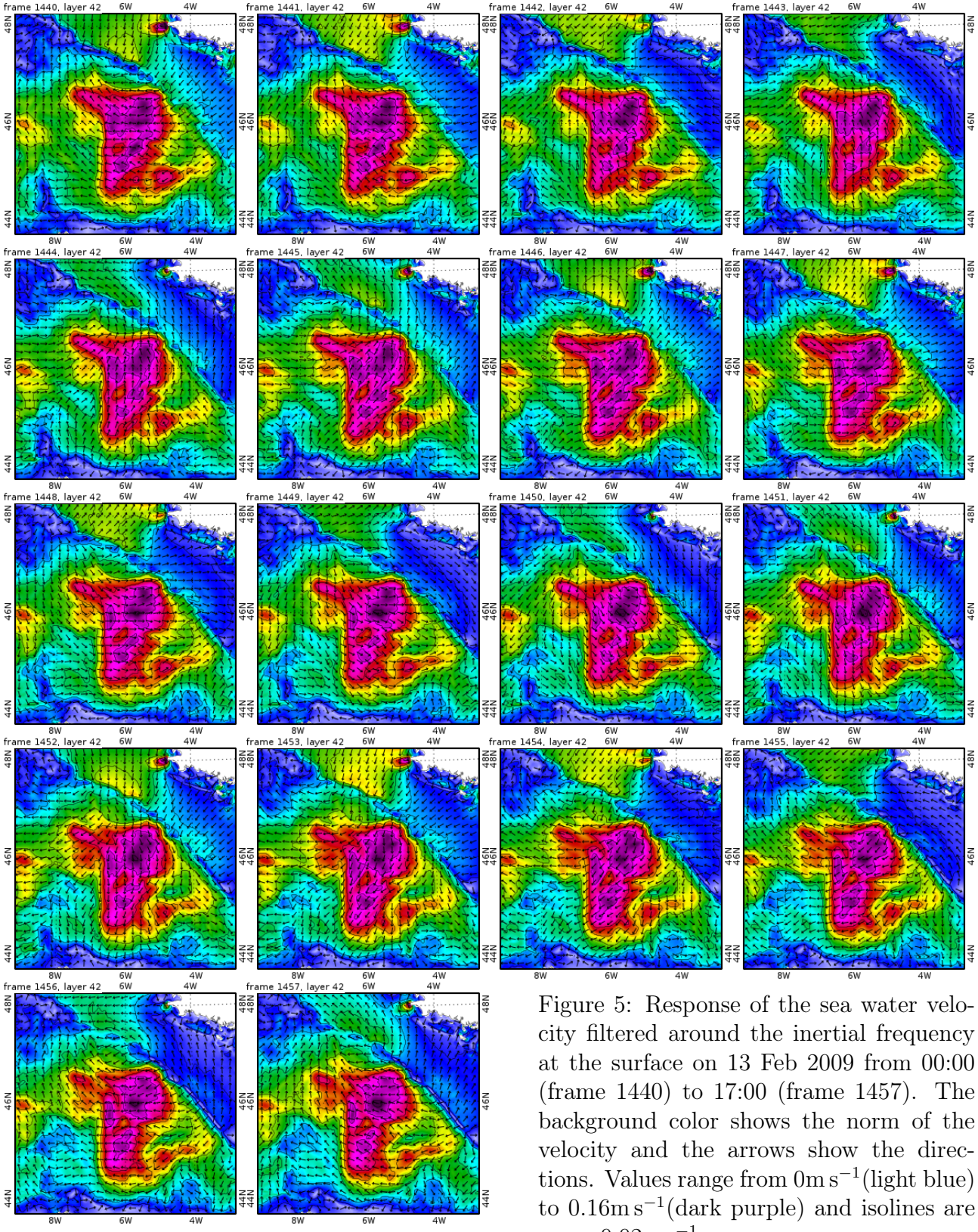

Figure 5: Response of the sea water velocity filtered around the inertial frequency at the surface on 13 Feb 2009 from 00:00 (frame 1440) to 17:00 (frame 1457). The background color shows the norm of the velocity and the arrows show the directions. Values range from $0\,\mathrm{m\,s^{-1}}$ (light blue) to $0.16\,\mathrm{m\,s^{-1}}$ (dark purple) and isolines are every $0.02\,\mathrm{m\,s^{-1}}$.

ocean values will be described here. Values at the boundaries of the model are particularly low. This shows the model was not forced with inertial waves at its open boundary. The values are particularly similar between the components.

There is a strong vertical gradient at 200 m of depth: all values above $0.03\,\mathrm{m\,s^{-1}}$ are above that depth and below that depth, most values are around $0.015\,\mathrm{m\,s^{-1}}$. All values above

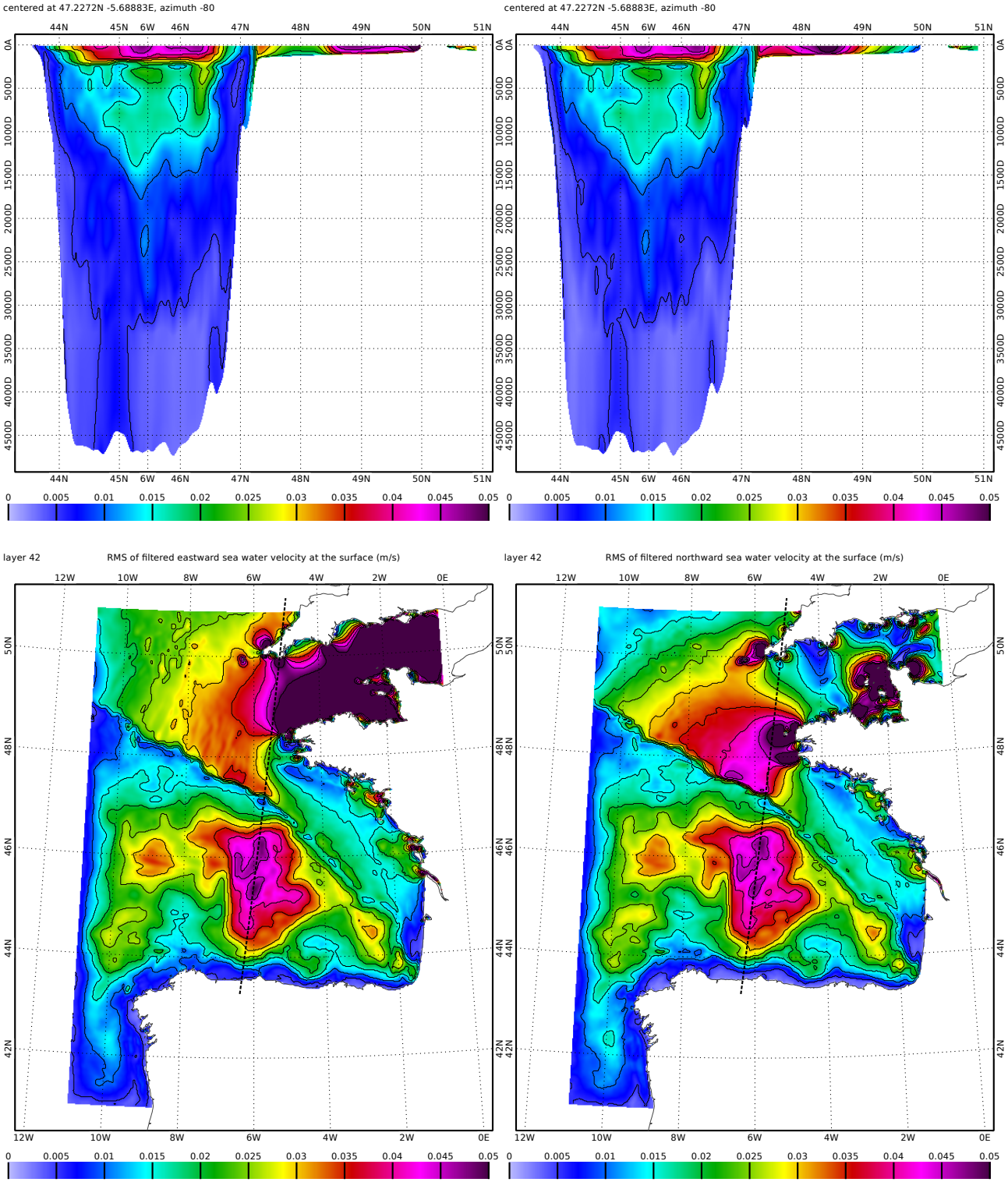

Figure 6: RMS of the eastward (left) and northward (right) components of the sea water velocity filtered around the inertial frequency, normalised by the RMS of the impulse response. Vertical view (top) and horizontal view of the surface layer (bottom). The thick dashed line shows the position of the vertical view.

$0.04\mathrm{m\,s^{-1}}$are in one area between 7W and 4.5W and north of 44.5N.

The eastward component was found to have the maximum at a position of 45.3811N 6.01434W at the surface. The time series at this location was filtered with $Q = 11$, so $b_p \simeq 0.016$, so $l = 412$ as the filter is symmetric. As the sampling is hourly, this makes the convolution kernel 25 days long. The results, and their frequency analyses, of the model output, the detided

model output, with N2, M2 and S2 removed, and the filtered detided model output at this location are shown on fig. 7. Only frequencies above $10°h^{-1}$ have been shown as meteorological variations below this frequency are not relevant to this study.

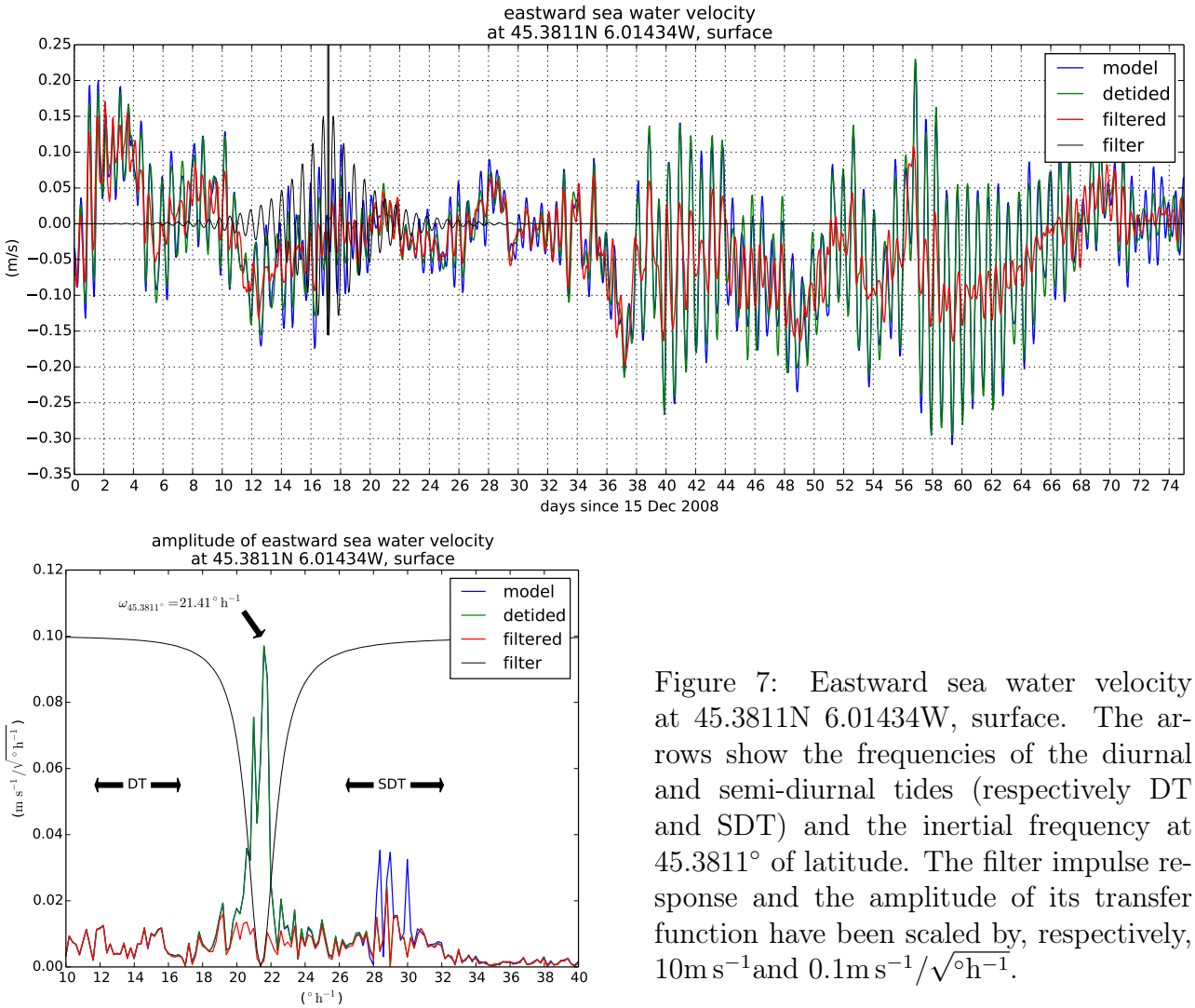

Figure 7: Eastward sea water velocity at 45.3811N 6.01434W, surface. The arrows show the frequencies of the diurnal and semi-diurnal tides (respectively DT and SDT) and the inertial frequency at 45.3811° of latitude. The filter impulse response and the amplitude of its transfer function have been scaled by, respectively, $10\,m\,s^{-1}$and $0.1\,m\,s^{-1}/\sqrt{°h^{-1}}$.

The frequency analysis of the model output shows a strong large peak between 20 and $22°h^{-1}$ with a maximum of $0.043\,m\,s^{-1}/\sqrt{°h^{-1}}$ at $21.6°h^{-1}$ which is very close to the the inertial frequency of $21.41°h^{-1}$. This peak is even larger than the peaks of the diurnal tides. There are 3 sharp peaks at the frequencies of semi-diurnal tides between 26.4 and $32°h^{-1}$. These peaks all reach between 0.014 and $0.016\,m\,s^{-1}/\sqrt{°h^{-1}}$ for N2 ($28.4°h^{-1}$), M2 ($29°h^{-1}$) and S2 ($30°h^{-1}$) tides. Otherwise, this analysis shows what can be interpreted as noise with most amplitude values below $0.006\,m\,s^{-1}/\sqrt{°h^{-1}}$ between $10°h^{-1}$ and $32°h^{-1}$ and all amplitude values below $0.002\,m\,s^{-1}/\sqrt{°h^{-1}}$ above $32°h^{-1}$. In particular, it shows no particular peak at the frequencies of diurnal tides between 11.7 and $16.7°h^{-1}$. The frequency analysis of the detided model output has only few differences with that of the model output. Only the peaks of the diurnal tides have been removed, although their remains a sharp peak just below the N2 frequency ($29°h^{-1}$) that reaches less than $0.011\,m\,s^{-1}/\sqrt{°h^{-1}}$. In particular, the IWs peak is preserved by the detiding as the frequencies given to the detidor were far from its frequency domain. The frequency analysis of the filtered detided model output has only few differences with that of the detided model output. Only the IWs peak has been removed, reducing the values in its frequency domain to levels very similar to the noise around.

What these frequency analyses show explains most of what what the results show. The

model output shows low frequency variations and some strong high frequency oscillations especially during the second half of the presented series. This particular part, from day 38, i.e. 22 Jan, starts with 6 days of oscillations with an amplitude around $0.15\,\mathrm{m\,s^{-1}}$followed by 8 days around $0.1\,\mathrm{m\,s^{-1}}$then, from 5 feb, by 5 days of oscillations with an amplitude around $0.15\,\mathrm{m\,s^{-1}}$then by 6 days of oscillations with an amplitude around $0.2\,\mathrm{m\,s^{-1}}$then finally decaying to less than $0.1\,\mathrm{m\,s^{-1}}$in the last 12 days.

The detided model output shows only small differences with the model output, in particular preserving the high frequency oscillations. The filtered detided model output removes most of the strong oscillations while preserving the low frequency variations. It does particularly well during the last quarter of the presented series, see the peak of day 56, i.e. 9 Feb, the day of the Quinten storm, but not so well during the first 10 days, when it only halfes the oscillations. This is because the filter is symmetric and therefore half of its convolution kernel sees almost no oscillation.

These results show that the filter can remove a lot of the signal from IWs but that a good understanding of the filter is necessary to interpret its output.

4.2 Synthetic case

In order to improve the understanding of the reader, a synthetic case is also presented fig. 8. The synthetic case also lasts 75 days. It starts at a value of $0.2\,\mathrm{m\,s^{-1}}$with a smooth transition

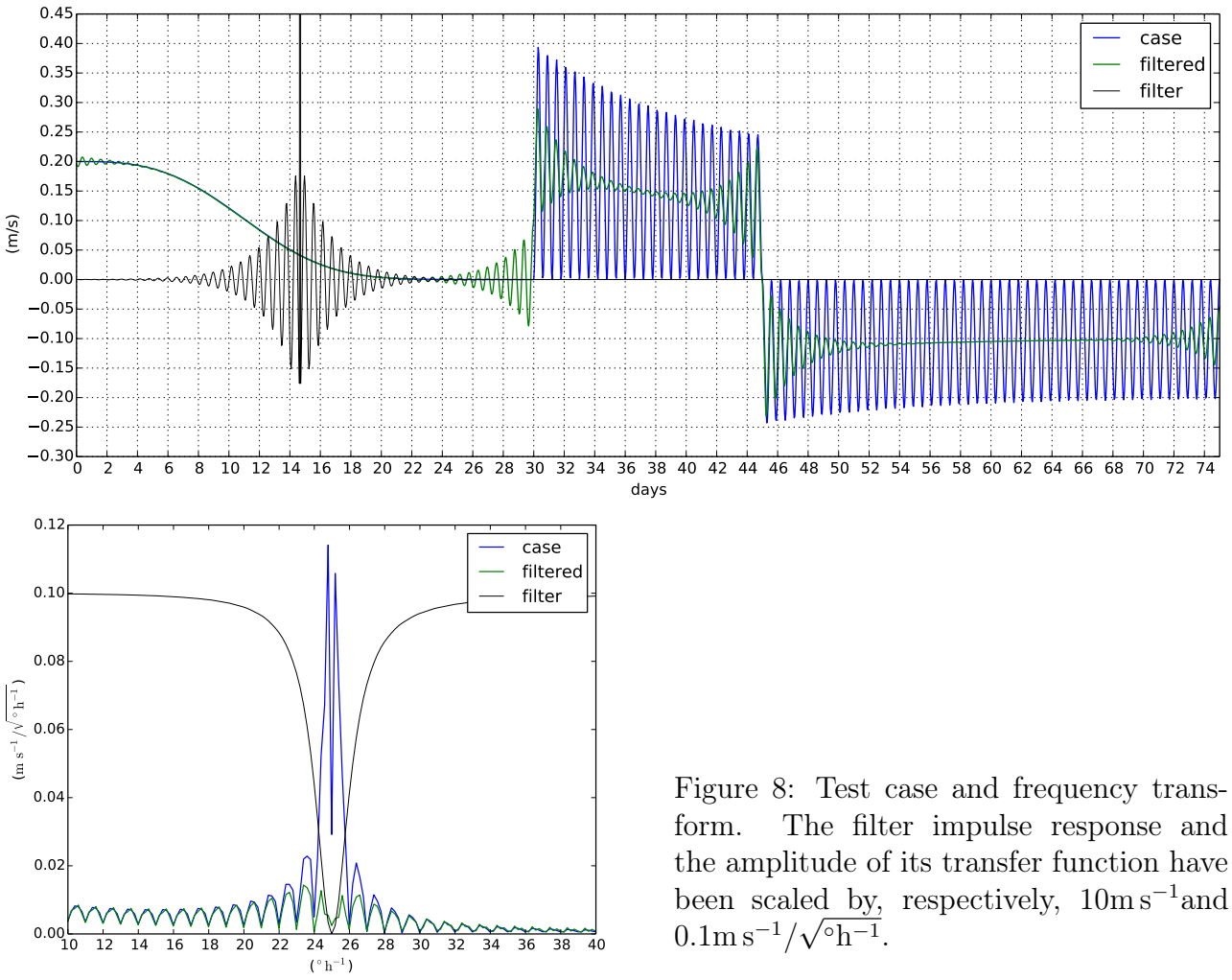

Figure 8: Test case and frequency transform. The filter impulse response and the amplitude of its transfer function have been scaled by, respectively, $10\,\mathrm{m\,s^{-1}}$and $0.1\,\mathrm{m\,s^{-1}}/\sqrt{^\circ\mathrm{h}^{-1}}$.

to $0\,\mathrm{m\,s^{-1}}$over less than 25 days. From day 30 to the end, the case oscillates at $25^\circ\mathrm{h}^{-1}$. The case oscillates between $0\,\mathrm{m\,s^{-1}}$and $0.4\,\mathrm{m\,s^{-1}}$decaying to $0.25\,\mathrm{m\,s^{-1}}$at day 44. On day 45, the sign

is inverted. From day 45 to the end, the case oscillates between $0\,\mathrm{m\,s^{-1}}$and -$0.25\,\mathrm{m\,s^{-1}}$decaying to -$0.2\,\mathrm{m\,s^{-1}}$at day 75. It must be noted that the case shows oscillations of almost $0.01\,\mathrm{m\,s^{-1}}$of amplitude on day 1, decaying to almost 0 on day 10. The filtered case shows oscillations from around day 22, increasing from $0\,\mathrm{m\,s^{-1}}$to $0.1\,\mathrm{m\,s^{-1}}$of amplitude on day 30, then decreasing to $0.004\,\mathrm{m\,s^{-1}}$on day 37 then increasing to $0.22\,\mathrm{m\,s^{-1}}$at the sign invertion on day 45 then decreasing to $0\,\mathrm{m\,s^{-1}}$on day 56. The filtered case also shows oscillations from around day 65, increasing from $0\,\mathrm{m\,s^{-1}}$to $0.05\,\mathrm{m\,s^{-1}}$on day 75.

This illustrates transition and boundary effects of the filter. There are small oscillations on step responses. The filter only halves input oscillations when they start and finish, because the filter is symmetric and therefore half of its convolution kernel sees no oscillation. The filter does not attenuate any oscillation around a sign invertion, because the filter is symmetric and therefore half of its convolution kernel sees oscillations one way and the other half sees oscillations the other way, but sign invertions will be most unlikely on real cases.

5 Conclusion

Symmetric filters have been designed to filter geophysical time series. As the symmetric filters are based on IIR digital filters, their computational costs are reduced to a minimum and their parameters can be adapted to all latitudes when used on IWs. The SBC filter has been tested. The results show that the SBC filter can remove a lot of the signal from IWs but that a good understanding of the filter is necessary to interpret its output, as it shows transition and boundary effects. For that reason, a synthetic case has been presented to enable users to get the best understanding of the filter.

Acknowledgements

I am grateful to Gaëlle Herbert for her model outputs. This work was funded by SHOM.

Bibliography

M. A. Demerliac. Calcul du niveau moyen journalier. *Annales hydrographiques du SHOM*, 2: 49–57, 1974. 2.1, 3

Gaëlle Herbert. *Modélisation et observation de la dynamique haute fréquence de la circulation du golfe de Gascogne*. PhD thesis, 2012. URL `http://thesesups.ups-tlse.fr/1751`. Downloaded 4 Jul 2014. 4.1

Claude Millot. The Gulf of Lions' hydrodynamics. *Continental Shelf Research*, 10(9–11):885–894, September 1990. doi: 10.1016/0278-4343(90)90065-T. URL `http://dx.doi.org/10.1016/0278-4343(90)90065-T`. Downloaded 11 Jun 2014. 1

A. Petrenko, C. Dufau, and C. Estournel. Barotropic eastward currents in the western Gulf of Lion, north-western Mediterranean Sea, during stratified conditions. *Journal of Marine Systems*, 74:406–428, November 2008. doi: 10.1016/j.jmarsys.2008.03.004. URL `http://dx.doi.org/10.1016/j.jmarsys.2008.03.004`. Downloaded 11 Jun 2014. 1

Julius O. Smith. *Introduction to Digital Filters with Audio Applications*. W3K Publishing, 2007. ISBN 978-0-9745607-1-7. URL `http://ccrma.stanford.edu/~jos/filters/`. Downloaded 30 Mar 2012. 2.1, 1, 6